[CANCER RESEARCH 61, 4561–4568, June 1, 2001]

Atm Knock-in Mice Harboring an In-frame Deletion Corresponding to the Human *ATM* 7636del9 Common Mutation Exhibit a Variant Phenotype[1]

Kevin Spring, Simone Cross, Chung Li, Dianne Watters, Liat Ben-Senior, Paul Waring, Farida Ahangari, Shan-li Lu, Philip Chen, Ihor Misko, Carol Paterson, Graham Kay, Nechama I. Smorodinsky, Yosef Shiloh, and Martin F. Lavin[2]

Queensland Cancer Fund Research Laboratories [K. S., S. C., D. W., F. A., P. C., I. M., C. P., G. K., M. F. L.] and Leukaemia Foundation of Queensland Research Laboratories [C. L., S-l. L.], The Queensland Institute of Medical Research, Herston, Brisbane, Queensland 4029, Australia; Hybridoma Unit, George S. Wise Faculty of Life Sciences [L. B-S.], and Department of Human Genetics, Sackler School of Medicine [N. I. S., Y. S.], Tel Aviv University, Ramat Aviv 69978, Israel; Department of Pathology, University of Melbourne, Parkville, Victoria 3052, Australia [P. W.]; and Department of Surgery, University of Queensland, Herston, Brisbane, Queensland 4029, Australia [M. F. L.]

ABSTRACT

***ATM*, the gene mutated in the human immunodeficiency disorder ataxia-telangiectasia (A-T), plays a central role in recognizing ionizing radiation damage in DNA and in controlling several cell cycle checkpoints. We describe here a murine model in which a nine-nucleotide in-frame deletion has been introduced into the *Atm* gene by homologous recombination followed by removal of the selectable marker cassette by Cre-loxP site-specific, recombination-mediated excision. This mouse, *Atm*-ΔSRI, was designed as a model of one of the most common deletion mutations (7636del9) found in A-T patients. The murine *Atm* deletion results in the loss of three amino acid residues (SRI; 2556–2558) but produces near full-length detectable *Atm* protein that lacks protein kinase activity. Radiosensitivity was observed in *Atm*-ΔSRI mice, whereas the immunological profile of these mice showed greater heterogeneity of T-cell subsets than observed in $Atm^{-/-}$ mice. The life span of *Atm*-ΔSRI mice was significantly longer than that of $Atm^{-/-}$ mice when maintained under nonspecific pathogen-free conditions. This can be accounted for by a lower incidence of thymic lymphomas in *Atm*-ΔSRI mice up to 40 weeks, after which time the animals died of other causes. The thymic lymphomas in *Atm*-ΔSRI mice were characterized by extensive apoptosis, which appears to be attributable to an increased number of cells expressing Fas ligand. A variety of other tumors including B-cell lymphomas, sarcomas, and carcinomas not seen in $Atm^{-/-}$ mice were observed in older *Atm*-ΔSRI animals. Thus, expression of mutant protein in *Atm*-ΔSRI knock-in mice gives rise to a discernibly different phenotype to $Atm^{-/-}$ mice, which may account for the heterogeneity seen in A-T patients with different mutations.**

INTRODUCTION

The human genetic disorder A-T[3] is characterized by immunodeficiency, neurodegeneration, sensitivity to ionizing radiation, and cancer predisposition (1, 2). Chromosomal instability in this disease is characterized by abnormal rearrangements involving chromosomes 7 and 14 in the vicinity of the TCR and immunoglobulin genes (3, 4). It has been suggested that a reduced capability in processing double-strand breaks in DNA is responsible for the radiosensitivity, immunodeficiency, infertility, and cancer predisposition (5, 6). Evidence in support of this has been provided by disruption of the *Atm* gene in mice. These animals developed malignant thymic lymphomas by 4–5 months of age (7–9), and these lymphomas had translocations in chromosome 14 occurring in both alleles of the TCR α/β locus (10). These data suggest that breaks occurring within the TCR locus during T-cell development undergo inappropriate end-joining, giving rise to genome instability and cancer predisposition. Consistent with this, Liao and Van Dyke (11) failed to observe the development of thymic lymphomas in $Atm^{-/-}$ $Rag1^{-/-}$ mice in which V(D)J recombination had been disrupted. On the other hand, Petiniot *et al.* (10) reported a lower frequency and longer latency period for thymic lymphomas in $Atm^{-/-}$ $Rag2^{-/-}$ mice compared with $Atm^{-/-}$ mice. Overall, the results point to an important but nonessential role for V(D)J recombination in tumorigenesis in *Atm*-deficient thymocytes (10).

The phenotype observed in $Atm^{-/-}$ mice generally reflects that seen in A-T patients with the exception of neurodegeneration, where the majority of studies failed to reveal such abnormalities (7–9, 12). In two cases, some evidence for neuronal degeneration and abnormal development of Purkinje cells was provided in $Atm^{-/-}$ mice (13, 14). In all of the $Atm^{-/-}$ mice generated to date, the disruption of the gene was achieved by means of gene inactivation leading to complete loss of *Atm* protein expression (7–9, 12, 14). Mice on either inbred or mixed genetic backgrounds did not show any phenotypic variation (7). Disruption of *Atm* led to a smaller size at birth, body weights of these mice were reduced during the early growth period, and fibroblasts from these animals grew poorly (7–9). Although the architecture of various lymphoid tissues was normal in $Atm^{-/-}$ mice, these organs were generally smaller in size (7–9).

Although there are clear hallmarks that characterize the A-T phenotype, some variability exists in these features (1), which might be explained by the nature of the mutation or genetic background. In addition to a phosphatidylinositol 3-kinase domain, the ATM protein contains several regions that interact with other proteins or are predicted to be functionally important (15, 16). Furthermore, there is evidence for a dominant-negative effect of a region of the ATM protein containing a putative leucine zipper motif (17). Because up to 20% of A-T patients express mutant protein and none of the $Atm^{-/-}$ mice produced to date express Atm protein, it was important to generate a mouse expressing mutant Atm protein and to determine whether these mice display any variation in the characteristics associated with the A-T phenotype. Accordingly, we produced mice homozygous for a nine-nucleotide in-frame deletion (7666del9) in *Atm*, which was predicted to give rise to a protein with three amino acids deleted (SRI; 2556–2558). This mutant corresponds to one of the most common A-T mutations found to date (15, 18). We report here that the phenotype of *Atm*-ΔSRI mice is significantly different to that described for $Atm^{-/-}$ mice.

MATERIALS AND METHODS

Gene Targeting and Generation of *Atm*-ΔSRI Mice. To generate a mutant mouse model of the human 7636del9 mutation found in A-T patient AT1ABR (15, 18), we used homologous recombination and the Cre-loxP system to introduce a nine-nucleotide in-frame deletion into exon 54 of mouse *Atm* (19). The gene targeting vector was constructed using a 5.5-kb *Eco*RV-

Received 12/11/00; accepted 4/2/01.

The costs of publication of this article were defrayed in part by the payment of page charges. This article must therefore be hereby marked *advertisement* in accordance with 18 U.S.C. Section 1734 solely to indicate this fact.

[1] Supported by funds from the Australian National Health and Medical Research Council, the A-T Medical Research Foundation, and the A-T Children's Project.

[2] To whom requests for reprints should be addressed, at The Queensland Cancer Fund Research Unit, The Queensland Institute of Medical Research, P. O. Box Royal Brisbane Hospital, Herston, Brisbane, Queensland 4029, Australia. Phone: 617-3362-0341; Fax: 617-3362-0106; E-mail: martinL@qimr.edu.au.

[3] The abbreviations used are: A-T, ataxia-telangiectasia; TCR, T-cell receptor; mAb, monoclonal antibody; ISEL, *in situ* end-labeling; ES, embryonic stem; SP, single positive; DP, double positive; SPF, specific pathogen-free; FasL, Fas ligand; IL, interleukin.

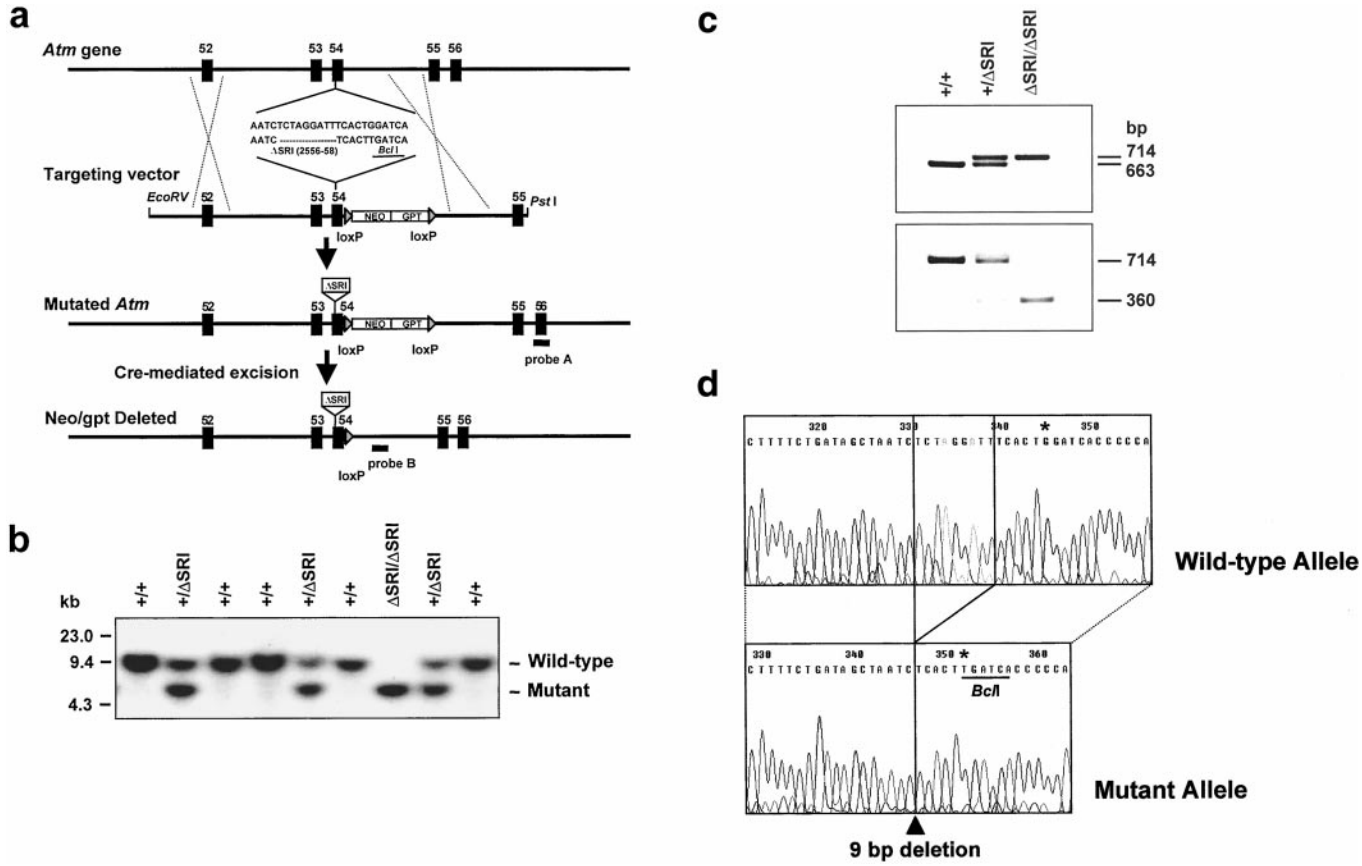

Fig. 1. Strategy used to mutate the mouse *Atm* via gene targeting. *a*, wild-type *Atm* with exons 52–56 marked and the targeting vector after mutating nucleotides 7666–7674 to introduce a nine-nucleotide deletion within exon 54. The position of the floxed *neo/gpt* cassette in intron 54 is also shown. Mutated *Atm* was detected in ES cells after digestion with *Eco*RV and DNA blot analysis using probe A. Deletion of the *neo/gpt* cassette in offspring from mating *Atm*-ΔSRI heterozygous mice with EIIa-Cre deleter mice was detected by *Pst*I digestion and hybridization with probe B. *b*, Southern blot analysis of tail tip DNA prepared from wild-type (+/+), *Atm*-ΔSRI heterozygous (+/Δ*SRI*), and *Atm*-ΔSRI homozygous (Δ*SRI*/Δ*SRI*) mutant mice. DNA was digested with *Eco*RV and probed with probe A. The expected size of the *Eco*RV fragments detected by probe A are 9.2 and 5.9 kb for the wild-type and mutant alleles, respectively. *c*, PCR and restriction-digestion analysis of tail DNA from +/+, +/ΔSRI, and ΔSRI/ΔSRI *Atm*-ΔSRI mice. Primers flanking exon 54 amplify either a wild-type 663-bp fragment or a mutated 714-bp fragment encompassing the nine-nucleotide deletion, *Bcl*I restriction site, and single loxP sequence residing in intron 54 (*top panel*). *Bcl*I restriction digestion of the genomic PCR products results in cleavage of the mutated allele fragment to two bands of 354 and 360 bp (*bottom panel*). *d*, sequence analysis of PCR fragments derived from wild-type and homozygous *Atm*-ΔSRI mice. Shading, the nine nucleotides deleted in the mutant *Atm* allele; *, nucleotide substitution used to create the *Bcl*I site.

*Pst*I genomic fragment isolated from a λZAP2 clone containing a mouse *Atm* insert derived from 129/SvJ genomic DNA (λDA1.1). On the basis of the mouse *Atm* cDNA sequence, removal of nucleotides 7666–7674 resulted in deletion of three amino acid residues (SRI; 2556–2558) at a position corresponding to the human 7636del9 mutation from patient AT1ABR. Site-directed mutagenesis was used to introduce this mutation into exon 54.

A 36-bp mutagenesis primer (5′-CTGATAGCTAATCTCACTTGATCACCCCCATCATAC-3′) was used to delete nucleotide 7666–7674 and also to create a novel *Bcl*I restriction site neutral polymorphism at nucleotides 7680. This restriction site was included as a marker to track the deletion mutation. A second 29-bp mutagenesis primer (5′-GTAACTGCAAGGGCCCTTTTGTGTTGTG-3′) was also used to introduce a unique *Apa*I site within intron 54, into which a loxP-*neo/gpt*-loxP selection cassette was inserted (Fig. 1). After transfection into 129SvJ ES cells (C1368) and G418 selection, two independently targeted clones were injected into C57BL/6J blastocysts, and 10 high-grade chimeric males were produced. These were, in turn, backcrossed with C57BL/6J, and of these, 8 transmitted the mutation through the germ line. The floxed *neo/gpt* selection marker was removed subsequently by crossing heterozygotes with the EIIa-Cre deleter mouse strain (20). The Cre-deleted mutant *Atm* mice were maintained on a 129/SvJ:C57BL/6J background. Mice generated by intercrossing heterozygotes were genotyped by Southern blot and PCR analysis at postnatal day 10. Tail tip DNA was extracted using proteinase K digestion and NaCl precipitation. Southern blotting was carried out by standard procedures. PCR genotyping was performed using forward (5′-TCTCATGTATCAATTGGCTGCTGC-3′) and reverse (5′-AATTGTTAACCAATTCTGGGTGGC-3′) primers to amplify exon 54 (wild-type 663-bp and mutant 714-bp fragments). Cycling conditions were 94°C for 12 min, 94°C for 1 min, 58°C for 1 min, and 72°C for 2 min over 35 cycles and analyzed on 1.2% agarose gels.

Mouse Growth Determinations and Survival. Mice were weighed at 7-day intervals beginning at postnatal day 10 to day 45 of age. After weaning, mice were divided by gender, and both food and water were provided *ad libitum*. Analysis of survival time for wild-type $Atm^{-/-}$ (kindly provided by Philip Leder, Harvard University, Boston, MA) and *Atm*-ΔSRI was calculated from date of birth to date of death or date last known alive. In this study, 129SvEv inbred ($Atm^{-/-}$) and 129SvJ:C57BL/65 mixed background ($Atm^{-/-}$ and *Atm*-ΔSRI) mice were used. Mice exhibiting ill health or obvious tumor burden were killed, and the underlying morbidity was recorded as the cause of death. Kaplan-Meier survival curves were generated for death attributable to tumors of either thymic or other tumor types, using the SPSS statistical package. Statistical significance was measured using the log-rank test at the 0.05 level.

Flow Cytometry Analysis. Thymocytes and lymph node cells from wild-type $Atm^{-/-}$ and *Atm*-ΔSRI mice were immunophenotyped by surface immunofluorescent labeling and flow cytometry. Cells were disaggregated in RPMI 1640 containing 10% FCS, 2 mM glutamine, and 5.5×10^{-5} M 2-mercaptoethanol. Cells ($1.0–1.5 \times 10^5$) in 20 μl of PBS with 1% FCS were incubated at 4°C for 30 min with 2–4 μl of antimouse mAbs, washed once in PBS + 1% FCS, and then analyzed for three-color immunofluorescence (FITC, phycoerythrin, and TRIC) with a Becton Dickinson FACScan and CellQuest software (version 3.1f). Cells expressing surface CD3, CD4, CD8, CD62L, CD44, α/βTCR (Caltag Laboratories Inc., Burlingame, CA), Fas/CD95, FasL (PharMingen, San Diego, CA), and Annexin V-FITC (PharMingen) are presented as

a percentage of the total number of cells. Thymic lymphomas were disaggregated and analyzed in the same way.

Production of mAbs. The mAb MAT3-4G10/8 was raised against a peptide spanning positions 1967–1988 of murine Atm, to which a cysteine residue was added at the NH_2 terminus for coupling to keyhole limpet hemocyanin. Mice were immunized with 50 μg of antigen (total of six injections over 15 weeks), and the appearance of antigen-specific antibodies was monitored by ELISA based on the antigen peptide and then by immunoblotting of mouse tissue extracts and immunoprecipitation of Atm from these tissues. Hybridomas were established using standard methods, and antibody production was monitored as described above. Seventeen clones were finally stocked, and clone 4G10/8, which produces heavy chain IgG1, was used in this study. The antibody was purified using fast protein liquid chromatography over a HiTrap protein G column (Pharmacia Biotech) and dialyzed against PBS.

Western Blotting. Protein extracts were prepared from spleens by homogenization in TGN buffer [50 mM Tris (pH 7.5), 50 mM β-glycerophosphate, 150 mM NaCl, 10% glycerol, 1% Tween 20, 1 mM NaF, 1 mM Na_3VO_4, 1 mM phenylmethylsulfonyl fluoride, 2 μg/ml pepstatin, 5 μg/ml leupeptin, 10 μg/ml aprotinin, and 1 mM DTT] and centrifuged at 13,000 $\times$ *g* for 15 min. Protein concentrations were determined using the Bio-Rad DC protein assay kit according to the manufacturer's recommendations. Protein samples (100 μg) were separated on 5 or 10% denaturing gels and blotted onto Hybond-C (Amersham) nitrocellulose membranes. After blocking in 4% milk powder, 0.1% Tween 20, and PBS for at least 1 h, blots were incubated for 1 h at room temperature or overnight at 4°C with the relevant primary antibody. Immunoreactive bands were visualized with Renaissance chemiluminescence substrate and captured on Kodak XAR X-ray film. The primary antibodies used in this study were mouse mAb anti-Atm MAT3-4G10/8 and rabbit antiactin (Sigma Chemical Co.).

***In Vitro* Atm-Kinase Assay.** Atm-kinase activity was determined using the method described by Canman *et al.* (21). For whole cell lysate isolation, cells were lysed on ice in TGN buffer. After centrifugation at 13,000 $\times$ *g* for 15 min, 1 mg of extract was precleared with protein A-Sepharose beads. Atm was immunoprecipitated with Atm antibody (MAT3), and the kinase activity was determined.

Cell Survival. Thymi were dissected from mice, and thymocytes were disaggregated in RPMI 1640 (10^6/ml) as described above. Cells were incubated with or without IL-2 (60 μg/ml) at 37°C in an atmosphere of 5% CO_2 for 24 h. Cells were exposed to ionizing radiation (0–4 Gy), and cell viability was determined by adding 0.1 ml of 0.4% trypan blue to a 0.5-ml suspension (22). The number of viable cells was determined at 48 and 72 h after irradiation.

Induced Chromosome Aberrations. Cells were irradiated with 1 Gy of γ-rays. For G_2-phase cells, Colcemid (final concentration, 0.1 mg/ml) was added immediately after irradiation, 1–2 h before harvesting. The cells were treated for 15 min in 0.075 M KCl, fixed in methanol:glacial acetic acid, 3:1 (vol/vol), and spread on glass slides. The cells were then stained with Giemsa, and 50 metaphases were analyzed for each sample (22).

ISEL of Tumor Sections. Paraffin sections of thymoma from $Atm^{-/-}$ and *Atm*-ΔSRI mice were dewaxed, digested with pepsin, and subjected to ISEL, essentially as described by Ansari *et al.* (23) using Biotin-16-dUTP (Enzo Diagnostics) in the labeling mix. Incorporated biotin-dUTP was detected with horseradish peroxidase coupled to streptavidin (DAKO) and 3,3′-diaminobenzidine staining. The sections were counterstained with hematoxylin, mounted, and photographed using an Olympus BH2 microscope.

RESULTS

Generation of *Atm*-ΔSRI Mutant Mice Expressing Mutant Atm Protein. Because the Atm protein is a high molecular weight molecule containing several potential domains in addition to the kinase domain, it is important to establish whether the presence of mutant Atm protein influences the A-T phenotype. To date, all of the *Atm* mouse models produced result in *Atm* gene inactivation and a complete abrogation of Atm protein expression. We therefore generated mice homozygous for a nine-nucleotide in-frame deletion (7666del9) in *Atm* resulting in the loss of three amino acids (SRI; 2556–2558), hereafter referred to as *Atm*-ΔSRI. The strategy used to introduce the ΔSRI mutation into *Atm* included the insertion of a loxP-flanked

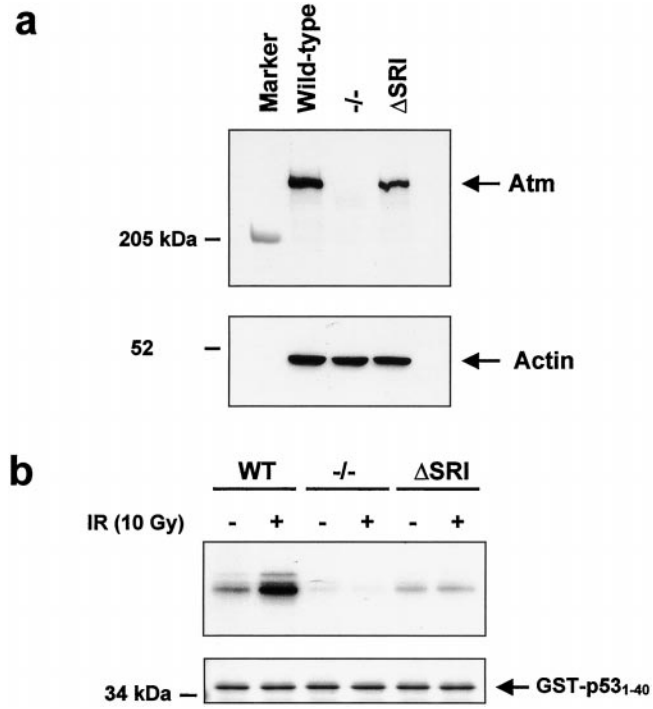

Fig. 2. Expression and activity of *Atm* protein in splenocytes from wild-type, $Atm^{-/-}$, and *Atm*-ΔSRI mice. *a*, immunoblotting of Atm protein (100 μg) was carried out using a mAb (MAT3) raised against a peptide corresponding to amino acids (1967–1988) of murine *Atm* (see "Materials and Methods"). Samples were separated on 4.5% SDS-PAGE prior to blotting, and protein loading was determined with an antiactin antibody. *b*, *Atm* kinase activity as determined by immunoprecipitation with anti-*Atm* (MAT3) antibodies. GST-p53$_{1-40}$ was used as a substrate. Extracts were prepared from unirradiated and irradiated (*IR*) cells (10 Gy) 1 h after exposure, and 1 mg immunoprecipitated with antibody prior to the kinase reaction. The amount of GST-p53$_{1-40}$ in each sample was determined by Coomassie staining. *WT*, wild type.

selectable marker cassette into the intron downstream of exon 54 (Fig. 1*a*; Ref. 24), which contains the nine-nucleotide deletion. Chimeric mice generated from two independently targeted 129SvJ ES cell clones (D11A and C9B) were crossed with C57BL/6J mice to produce *Atm*-ΔSRI heterozygotes. The loxP-selectable marker cassette was removed by crossing *Atm*-ΔSRI heterozygous mice with an EIIa-Cre deleter mouse strain that constitutively expresses Cre recombinase (20). *Atm*-mutant mice were identified by Southern blot analysis of tail tip DNA (Fig. 1*b*) or PCR analysis of a region containing the deletion mutation and *Bcl*I site (Fig. 1*c*, *top panel*). Using this analysis, it is possible to distinguish *Atm*-ΔSRI homozygotes (714 bp) from heterozygotes and wild type (663 bp). The increased size of the *Atm*-ΔSRI homozygous band is attributable to the presence of a single loxP site in intron 54. Cleavage with *Bcl*I confirmed the presence of the mutation (Fig. 1*c*, *bottom panel*). Deletion of the nine-nucleotide sequence was verified by genomic DNA sequencing (Fig. 1*d*). These ΔSRI mutant mice expressed near full-length Atm protein, whereas no Atm protein was detected in $Atm^{-/-}$ mice, as determined by immunoblotting of spleen cell extracts with a mAb (MAT 3) derived against the mouse Atm sequence (Fig. 2*a*). Because we have shown previously that the corresponding human mutant protein typified in the cell line AT1ABR (15, 18) is kinase-dead and thereby incapable of phosphorylation of p53 on serine 15 (25), we measured the kinase activity of *Atm*-ΔSRI splenocytes using p53$_{1-40}$ as a substrate as described previously (21, 26). A marked increase in Atm-kinase activity was observed in wild-type spleen cell extracts in response to radiation exposure, whereas only a low level of residual kinase activity, which did not respond to radiation, was observed in *Atm*-ΔSRI extracts (Fig. 2*b*). As expected, extracts from $Atm^{-/-}$ mice displayed no Atm-kinase activity.

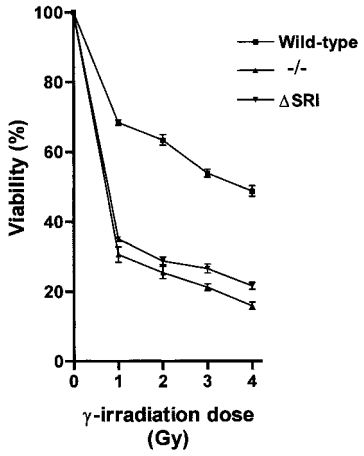

	Number of Aberrations			
Cell	sb	cb	int	ICA/metaphase
WT (50)*	45	0	0	0.9
-/- (25)	62	0	1	2.81
ΔSRI (50)	135	0	4	2.78

*** chromosome aberrations were analysed in number of metaphases as shown in parental. sb; chromatid break; cb, chromosome breaks; int, interchanges; ICA, induced chromosome aberrations. Cells were irradiated with 1 Gy.**

Fig. 3. Survival of thymocytes from wild-type, $Atm^{-/-}$, and *Atm*-ΔSRI (Δ*SRI*) mice in response to radiation. Thymocytes were isolated and incubated in medium supplemented with IL-2 (60 μg/ml) for 24 h before radiation exposure. *Top panel*, viability was determined by trypan blue exclusion at 48 and 72 h after irradiation. The viability data at 3 days after irradiation are depicted. *Bottom panel*, radiation-induced chromosome aberrations in wild-type, $Atm^{-/-}$, and *Atm*-ΔSRI thymocytes isolated and treated as described above. The radiation dose used was 1 Gy.

Growth and Other Defects in *Atm*-ΔSRI Mice. Previous data have revealed the presence of a growth defect in $Atm^{-/-}$ mice, which appears to be largely attributable to disruption of the gene *per se* (7–9). Consistent with these observations, growth retardation was seen both in male (20% reduction) and female (18% reduction) *Atm*-ΔSRI mice from birth to 45 days of age and persisting throughout adulthood. A-T cells and ES cells from $Atm^{-/-}$ mice have been shown to be hypersensitive to ionizing radiation (14, 27, 28). Incubation of freshly isolated thymocytes from *Atm*-ΔSRI and $Atm^{-/-}$ mice in the presence of IL-2 for 24 h before radiation exposure (1–4 Gy) resulted in significantly more cell death than observed with wild-type thymocytes at 48 h after irradiation (Fig. 3, *top panel*). There appeared to be somewhat less killing in the absence of IL-2, but thymocytes were still distinguishable from wild-type (results not shown). The extent of cell death was similar in *Atm*-ΔSRI and $Atm^{-/-}$ thymocytes. This was additionally confirmed by preparing metaphase chromosomes from irradiated thymocytes. The number of induced chromosome aberrations/metaphase was approximately one in wild-type thymocytes, whereas the number for *Atm*-ΔSRI and $Atm^{-/-}$ mice was approximately three times that value (Fig. 3, *bottom panel*). We also demonstrated enhanced radiosensitivity in splenocytes from *Atm*-ΔSRI and $Atm^{-/-}$ mice (data not shown). These data are comparable with the relative values observed in irradiated A-T and normal cells (22).

Although neurological abnormalities have been reported for $Atm^{-/-}$ mice, the majority of the evidence suggests that neurodegeneration is not present in these animals (7–9, 12), with the exception of two reports where degeneration of several different types of neurons in the cerebellar cortex of $Atm^{-/-}$ mice was evident from electron microscopic analysis, in one case (13), and in the other, where ectopic expression and abnormally differentiated Purkinje cells were apparent (14). As with $Atm^{-/-}$ mice, *Atm*-ΔSRI mice, 2–16 months of age, failed to show any evidence of gross neuronal degeneration, specific loss, or abnormal migration of Purkinje cells (results not shown). Similar to $Atm^{-/-}$ mice, there was also evidence of testicular abnormalities (poorly developed testes) and disruption of spermatogenesis in *Atm*-ΔSRI mice ($n = 2$). In contrast to seminiferous tubules of testes from wild-type mice where abnormalities were not observed, tubules from *Atm*-ΔSRI mice were disrupted with evidence of degeneration of spermatocytes and loss of spermatids (Fig. 4, *a* and *b*). Similarly, oogenesis in *Atm*-ΔSRI mice ($n = 2$) was disrupted with an observed lack of maturing follicles and oocytes (results not shown).

Immunological Abnormalities in *Atm*-ΔSRI Mice. A variable but common characteristic in A-T is immunodeficiency and immune defects, which are reproduced in $Atm^{-/-}$ mice. To characterize the T-cell development/phenotype in *Atm*-ΔSRI mice, cell samples of thymus and inguinal lymph node were analyzed by flow cytometry and compared with those from age-matched (7–12 weeks) wild-type and $Atm^{-/-}$ mice. *Atm*-ΔSRI mice had smaller thymi, spleens, and lymph nodes than wild-type mice and 10 times fewer thymocytes than wild-type mice, in agreement with data for $Atm^{-/-}$ mice. A reduction of 30–50% in the total number of thymocytes expressing α/βTCR and CD3 was observed in the thymi of $Atm^{-/-}$ and *Atm*-ΔSRI mice, which is consistent with previous results for $Atm^{-/-}$ mice (9). More detailed analysis of eight 12-week-old *Atm*-ΔSRI mice revealed that three of these mice showed significant increases in cell size, as reflected in scatter analysis and apparently random accumulation of either $CD4^{-/Low}$ $CD8^{-/Low}$ (60%), $CD8^{+}$ (39%), or $CD4^{+}$ (64%) SP populations. This heterogeneity in three *Atm*-ΔSRI mice is illustrated in Fig. 5*a*. These changes in T-cell subtypes were also evident in two younger (8-week) *Atm*-ΔSRI mice. On the other hand, $Atm^{-/-}$ mice more closely resembled the wild type in the proportions of DP and SP T cells.

The lymph nodes of $Atm^{-/-}$ mice contain only 50% of lymphocytes expressing either CD3, $CD4^{+}CD8^{+}$, and CD62L or CD44 compared with *Atm*-ΔSRI and wild-type mice (results not shown). On the basis of the combination of low CD3, low CD62L, and low CD44 expression, the $Atm^{-/-}$ lymph nodes appear to consist primarily of T cells at an early stage of development (29). Both CD62L and CD44 are putative markers for memory T cells in mice.

Life Span, Thymic Lymphomas, Apoptosis, and Up-Regulation of FasL in *Atm*-ΔSRI Mice. Patients with A-T have been demonstrated to develop a spectrum of tumors, primarily leukemias and lymphomas (6). On the other hand, $Atm^{-/-}$ mice develop exclusively malignant thymic lymphomas and die between 2 and 5 months of age when held in non-SPF facilities (7–9, 28). In this study (under non-SPF conditions), the life span of *Atm*-ΔSRI mice ($n = 43$) was increased dramatically compared with $Atm^{-/-}$ mice ($n = 26$). When 100% of $Atm^{-/-}$ mice were dead, only 50% of *Atm*-ΔSRI animals had

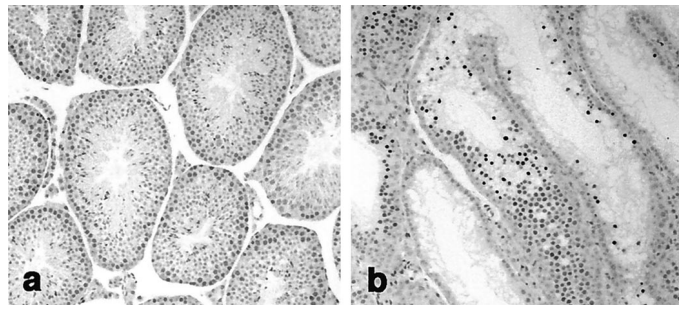

Fig. 4. Effect of Atm disruption on reproductive capability. H&E-stained sections through seminiferous tubules from wild-type (*a*) and *Atm*-ΔSRI mice (*b*). ×40.

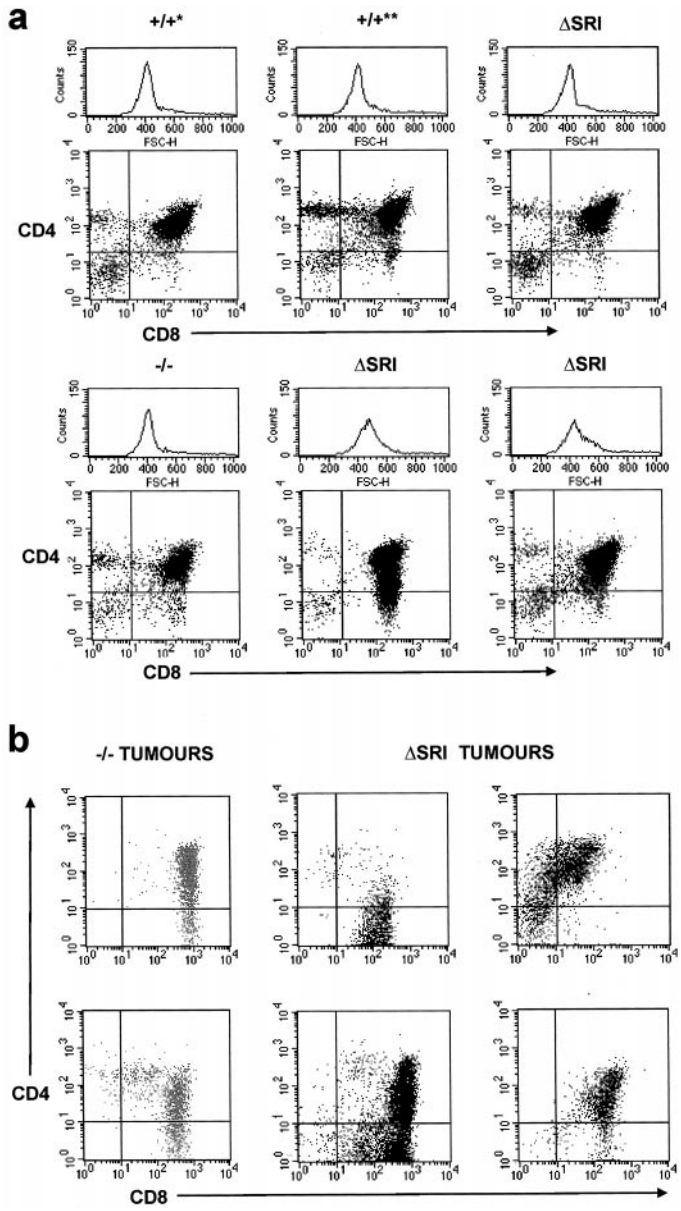

Fig. 5. FACS analysis of T-cell surface antigen expression in normal thymocytes and thymic lymphomas. *a*, forward scatter analysis (*top panel*) of thymocytes from wild-type, *Atm* $^{-/-}$, and *Atm*-ΔSRI mice. *Bottom panel*, surface expression for CD4 and CD8 T-cell populations. *Top right quadrants*, double-positive cell populations. *b*, surface expression of CD4 and CD8 on thymic lymphomas from *Atm* $^{-/-}$ and *Atm*-ΔSRI mice.

died (Fig. 6). At this stage, autopsies revealed the presence of thymic lymphomas in all of these animals, indicating that death was a consequence of malignancy. Almost 30% of *Atm*-ΔSRI mice were alive after 16 months. The results obtained here for $Atm^{-/-}$ mice are consistent with previous reports on survival of these animals (9, 30). Difference in survival appears not to be attributable to genetic background because both types of mice used here were of mixed genetic background: (*a*) C57BL/6J crossed with 129SvJ for *Atm*-ΔSRI; and (*b*) C57BL/6J crossed with 129SvEv for $Atm^{-/-}$. Differences between 129Sv substrains do not significantly affect tumor incidence (31), and previous results have failed to demonstrate phenotype variance between mixed and inbred backgrounds for $Atm^{-/-}$ mice (7).

Phenotypic analysis of the thymic lymphomas revealed that the $Atm^{-/-}$ phenotype was characterized predominately by $CD4^+CD8^+$ DP cells and low CD3 (data not shown), whereas the *Atm*-ΔSRI lymphomas were more diverse, reflecting the greater heterogeneity of DP and SP populations of T cells seen in the thymi of these animals and may represent polyclonal tumors (Fig. 5*b*).

Morphological examination of thymic lymphomas from *Atm*-ΔSRI mice (>3 months of age) revealed that these tumors were more spongy and the cells less tightly aggregated than in the $Atm^{-/-}$ tumors. Histological examination of tumors showed that there was a significantly increased proportion of cells undergoing what appeared to be spontaneous apoptosis based on nuclear fragmentation in *Atm*-ΔSRI tumors (Fig. 7*b*) compared with $Atm^{-/-}$ tumors (Fig. 7*a*). These cells were confirmed as apoptotic by ISEL staining (Fig. 7, *c* and *d*), and ~50% of *Atm*-ΔSRI thymic lymphoma cells were Annexin V positive compared with ~15% in $Atm^{-/-}$ thymic lymphomas (results not shown). To investigate these differences, we isolated disaggregated cells from the two types of tumors as well as thymocytes from wild-type and from the *Atm*-disrupted mice and performed flow cytometric analysis to compare surface markers for susceptibility to undergo apoptosis (32). Down-regulation of the Fas receptor (Fas/CD95) was evident in thymocytes in both $Atm^{-/-}$ and *Atm*-ΔSRI mice, with 30–40% fewer Fas-positive cells than in wild type (Table 1). This pattern of down-regulation is also seen in thymic lymphomas

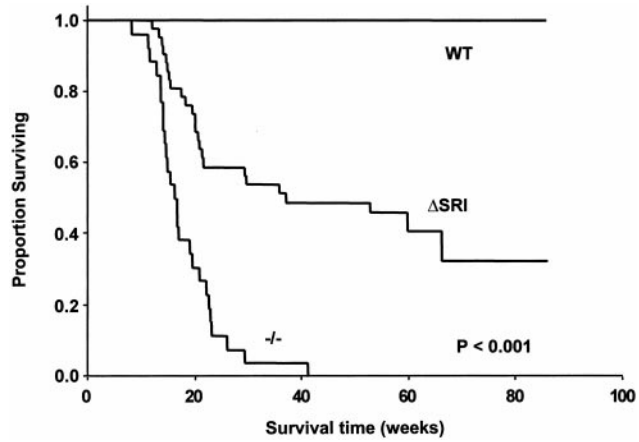

Fig. 6. Kaplan-Meier survival plot of wild-type (*WT*), Atm $^{-/-}$, and ΔSRI mice. *P* was calculated by comparing life spans of mice from each genotype using the SPSS statistical package. $Atm^{-/-}$ and *Atm*-ΔSRI mice of either 129Sv inbred or 129Sv:C57BL/6J mixed genetic background were used in this study. No differences in survival were observed with mice of different genetic backgrounds.

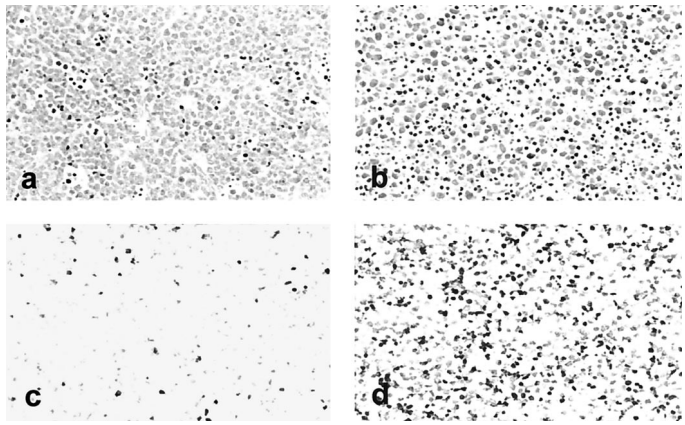

Fig. 7. Histological examination of thymic lymphomas. *a* and *b*, H&E staining of thymic lymphoma sections from *Atm* $^{-/-}$ and *Atm*-ΔSRI mice. ×40. The *Atm* $^{-/-}$ thymic lymphoma (*a*) shows a reduced nuclear fragmentation indicative of apoptosis as compared with the *Atm*-ΔSRI thymic lymphoma (*b*), which shows extensive apoptosis. *c* and *d*, ISEL of paraffin sections of thymic lymphomas from *Atm* $^{-/-}$ and *Atm*-ΔSRI mice. Cells were labeled with Biotin-16-dUTP, and apoptosis was detected with horseradish peroxidase-coupled streptavidin and 3,3′-diaminobenzidine.

Table 1 *Flow cytometric analysis of Fas and FasL in $Atm^{-/-}$ and Atm-ΔSRI thymic lymphoma*

Tissue and genotype[a]	Fas	FasL
Thymus		
Wild-type	90.6 ± 0.8[b]	3.0 ± 0.6
$Atm^{-/-}$	62.7 ± 2.4	2.8 ± 1.2
Atm-ΔSRI	54.8 ± 4.5	2.2 ± 0.4
Thymic lymphoma		
$Atm^{-/-}$	60.8 ± 7.7	7.5 ± 1.5
Atm-ΔSRI	57.8 ± 10.8	30.7 ± 0.9

[a] $n = \geq 5$ mice in each group.
[b] Percentage of total thymocytes ± SE.

from both forms of mutant mice. Expression of FasL was approximately the same in thymocytes from wild-type and mutant mice (Table 1). A small increase was evident in thymic lymphomas from $Atm^{-/-}$ mice, but in thymic lymphomas from *Atm*-ΔSRI mice there was an ~14-fold increase in the number of cells expressing FasL (Table 1). This corresponds well with the increased extent of apoptosis detected in thymic lymphomas from *Atm*-ΔSRI mice compared with $Atm^{-/-}$ mice. However, this extent of apoptosis was not observed, and FasL was not up-regulated in *Atm*-ΔSRI mice developing lymphomas at <2 months of age. To test the functionality of the FasL expression in *Atm*-ΔSRI tumors, we incubated thymic lymphoma cells with a target cell line AT1ABR, a lymphoblastoid cell line from a patient with A-T, containing the same mutation as in the *Atm*-ΔSRI mice (18). This cell line has a high expression of Fas.[4] At a ratio of 3:1 lymphoma:target cells, viability of AT1ABR was reduced by 80% after 12-h incubation demonstrating that the up-regulated FasL was active in the apoptotic process observed in *Atm*-ΔSRI tumors (results not shown). This was substantiated additionally by attempts to establish the tumor lines in culture, where it was observed that those from *Atm*-ΔSRI were more difficult to grow.

Development of a Spectrum of Tumors in Long-lived *Atm*-ΔSRI Mice. It is evident from the data in Fig. 6 that the longevity of *Atm*-ΔSRI mice is markedly greater than that of most $Atm^{-/-}$ mice. As indicated above, all of the $Atm^{-/-}$ mice had died from thymic lymphomas by 40 weeks in this study. The 44% (19 of 43) of *Atm*-ΔSRI mice that had died by the same time also died with the same tumors. Very few *Atm*-ΔSRI mice died after this time from thymic lymphomas, but a significant number of deaths (7) were associated with a variety of other tumors. Upon autopsy, the mice usually displayed marked splenomegaly but with minimal involvement of the thymus. Immunotyping showed that three of these animals had B-cell leukemia. The B-cell tumors grew aggressively with no evidence of FasL up-regulation. Furthermore, histopathological examination of various tissues/organs revealed the presence of multiple tumor types including ovarian granulosa cell tumors, epithelial carcinomas, histiocytic/reticulum cell tumors, ovarian sex cord, and stromal cell tumors. Mutant Atm protein was expressed in both lymphoid and solid tumors (results not shown).

DISCUSSION

The *Atm*-ΔSRI mouse represents a dysfunctional *Atm* model that expresses mutant protein unlike all of the other $Atm^{-/-}$ mice described to date, which do not express Atm protein because of the nature of the gene disruption (7–9, 12, 14). In one case, a *neo*^{r} gene replaced a portion of the Rad-3 homology domain of *Atm*, but neither full-length *Atm* transcript nor protein were detected (14). The mutant mouse described here corresponds to a commonly observed mutation in A-T patients (7636del9; Refs. 15 and 18). As with the human mutant, *Atm*-ΔSRI protein is less stable as judged by the amount of Atm determined by immunoblotting, and no Atm-kinase activity was detected, similar to that for the human mutant (33). However, some variability in the amount of *Atm*-ΔSRI protein was observed in different experiments. Because this short deletion is upstream from the kinase domain, it is likely that it causes an inactivating, conformational change in the Atm protein or prevents binding of a protein critical for activity. Since the SRI sequence is in a putative domain, FAT (Ref. 34; FRAP, ATM, and TRAPP), present in a subfamily of phosphatidylinositol 3-kinases, and because this domain is implicated in multimeric protein complex formation, its loss may interfere with protein-protein interactions. There is evidence that ATM is present in a large protein complex with BRCA1, BLM, Mrell-Rad50-NBS1, and DNA repair proteins, called BRCA1-associated genome surveillance complex (35), but none of these proteins have been shown to interact with this region of ATM.

In this study, thymocytes and splenocytes from both $Atm^{-/-}$ and *Atm*-ΔSRI mice were more susceptible to radiation-induced killing than wild-type cells. This was confirmed by radiation-induced chromosome aberrations, which were 3-fold higher in both types of mutant mouse thymocytes than in wild-type cells. This is in agreement with two previous reports that showed that ES cells from $Atm^{-/-}$ mice were hypersensitive to radiation at low doses (≥5 Gy; Refs. 14 and 28), although other reports suggest that $Atm^{-/-}$ cells are only equally as sensitive or even less sensitive than controls to ionizing radiation (12, 28, 30). However, at least in the case of embryonic fibroblasts, extremely poor growth makes it difficult to differentiate between the two cell types (7). Although Elson *et al.* (9) have shown that the relative extent of the increase in chromosome damage by bleomycin is similar in *Atm*-deficient and wild-type murine fibroblasts, the absolute value, 9.71 breaks/metaphase, is considerably greater in $Atm^{-/-}$ cells than in wild type (1.70 breaks/metaphase). This might very well translate into increased cell killing. Indeed, Westphal *et al.* (36) have shown that loss of *Atm* radiosensitizes multiple cell types including fibroblasts, bone marrow, and gastrointestinal cells as well as p53-null bone marrow cells. Furthermore, whereas $p53^{-/-}$ cells are considered generally to be radioresistant, mitogenic stimulation of $p53^{-/-}$ lymphocytes renders them susceptible to radiation-induced killing (37). In other studies, exposure conditions were different in that whole animal irradiation occurred prior to cell isolation, higher doses were used (5–20 Gy), and apoptosis was the end point (12, 28, 30, 36, 38). All of these studies point to reduced apoptosis in irradiated $Atm^{-/-}$ cells. However, because death by apoptosis may only account for 30% of radiation-induced killing in A-T cells (39), the data obtained may not reflect the actual extent of cell killing. In addition, Brown and Wouters (40) have reported that when clonogenic survival is used as an end point of cell killing, ability to undergo apoptosis does not contribute significantly to the sensitivity of tumor cells to radiation and chemotherapeutic drugs.

Although a number of the $Atm^{-/-}$ phenotypic characteristics have been reproduced in the *Atm*-ΔSRI mice, the most dramatic difference is the significantly greater life span of these animals. In the experiments conducted here, *Atm*-ΔSRI and $Atm^{-/-}$ mice were bred in a non-SPF facility. In previous reports, $Atm^{-/-}$ mice were also housed under non-SPF conditions, and all of the animals had died with thymic lymphomas between 2 and 5 months of age (7–9, 30). The $Atm^{-/-}$ mice used here died at rates comparable with those observed previously for these animals (9). Longer life spans in $Atm^{-/-}$ mice appear to be attributable to breeding in pathogen-free conditions. This is particularly evident with the $Atm^{-/-}$ mice produced by Barlow *et al.* (7), where the mice did not survive beyond 4.5 months, but when the same animals were maintained in SPF housing, 40% of animals were still alive after 18 months (10). Breeding was also carried out in

[4] I. Filippovich, unpublished observations.

pathogen-free facilities by Borghesani *et al.* (14), where 50% of *Atm* mutant mice were alive after 10 months. Clearly, SPF conditions were not required for the prolonged life span described here in *Atm*-ΔSRI mice.

The extent of apoptosis occurring in thymic lymphomas from *Atm*-ΔSRI mice may contribute to the longevity in *Atm*-ΔSRI mice. Previous studies have failed to observe apoptotic cells in tumors from the $Atm^{-/-}$ mice used in the present investigation (41). However, thymic lymphomas derived from *Atm*/*p21* double-null mice show high levels of apoptotic cells. It appears likely that loss of p21 potentiates the apoptotic response presumably because of a lack of G_2 arrest (41). It seems likely that the increased apoptosis seen here in *Atm*-ΔSRI tumors is attributable to up-regulation of FasL. Interaction of FasL with the death receptor Fas is responsible for the subsequent assembly of a death-inducing signaling complex, which in turn activates caspase-8 and other downstream caspases leading to cell death (42, 43). FasL is up-regulated to prevent uncontrolled T-cell expansion and cytokine production (44) but can also be up-regulated by a variety of other agents including ionizing radiation (45), reactive oxygen species, IFNs, tumor necrosis factor-α (46, 47), and nuclear factor-κB (48). An imbalance in any of these factors caused by the presence of mutant Atm could contribute to the FasL up-regulation. The increased expression of FasL in *Atm*-ΔSRI thymic lymphomas and consequent apoptosis may explain why only 50% of *Atm*-ΔSRI mice succumb to thymic lymphomas after 40 weeks, at which time all of the $Atm^{-/-}$ mice ($n = 26$) in this study had died from thymic lymphomas (Fig. 6). The "take rate" of these tumors may be reduced by Fas/FasL-induced apoptosis. In all, 19 of 43 (44%) of *Atm*-ΔSRI mice died of thymic lymphomas up to 10 months of age. Some of the other animals died from splenetic, ovarian, and B-cell tumors with evidence of metastatic spread. To date, no B-cell tumors have been recorded in $Atm^{-/-}$ mice, and there has been no evidence of tumor metastases in these mice. Whereas the *Atm*-ΔSRI mice have significantly increased longevity over the $Atm^{-/-}$ mice, it appears that there may be two periods of tumor susceptibility: (*a*) the initial period up to 10 months where animals develop thymic lymphomas; and (*b*) for the survivors, a later onset of tumorigenesis with a distinct set of tumors. This second period of tumor susceptibility can be explained by the development of age-related tumors. No tumors were observed in wild-type controls during the same time frame. Thus, the phenotype of the mutant described here provides additional evidence for heterogeneity in A-T, and it provides a model to investigate additionally the molecular basis of tumor development in A-T.

ACKNOWLEDGMENTS

We thank Dr. Glenda Gobe for helpful discussions, Dr. David Purdie for statistical analysis, Ella Harness and Margaret Yaakubowitz for expert technical help, and Ann Knight and Kylee Wallace for typing the manuscript. We also acknowledge the kind gift of $Atm^{-/-}$ from Dr. Philip Leder, Harvard University, Boston, MA.

REFERENCES

1. Sedgwick, R. P., and Boder, E. Hereditary neuropathies and spinocerebellar atrophies. *In:* J. M. B. Vianney De Jong (ed.), Handbook of Clinical Neurology, pp. 347–423. New York: Alan R. Liss, Inc., 1991.
2. McFarlin, D. E., Strober, W., and Walkman, T. A. Ataxia-telangiectasia. Medicine (Baltim.), *51:* 281–314, 1972.
3. Oxford, J. M., Harnden, D. G., Parrington, M., and Delhanty, J. D. A. Specific chromosome aberrations in ataxia-telangiectasia. J. Med. Genet., *12:* 251–262, 1975.
4. McCaw, B. K., Hecht, F., Harnden, D. G., and Teplitz, K. L. Somatic rearrangements of chromosome 14 in human lymphocytes. Proc. Natl. Acad. Sci. USA, *72:* 2071–2075, 1975.
5. Lavin, M., and Shiloh, Y. The genetic defect in ataxia-telangiectasia. Annu. Rev. Immunol., *15:* 177–202, 1997.
6. Taylor, A. M., Metcalfe, J. A., Thick, J., and Mak, Y. F. Leukemia and lymphoma in ataxia-telangiectasia. Blood, *87:* 4223–4438, 1996.
7. Barlow, C., Hirotsune, S., Paylor, R., Liyanage, M., Eckhaus, M., Collins, F., Shiloh, Y., Crawley, J. N., Reid, T., Tagle, D., and Wynshaw-Boris, A. Atm-deficient mice: a paradigm of ataxia-telangiectasia. Cell, *86:* 159–171, 1996.
8. Xu, Y., Ashley, T., Brainerd, E. E., Bronson, R. T., Meyn, M. S., and Baltimore, D. Targeted disruption of ATM leads to growth retardation, chromosomal fragmentation during meiosis, immune defects, and thymic lymphoma. Genes Dev., *10:* 2411–2422, 1996.
9. Elson, A., Wang, Y., Daugherty, C. J., Morton, C. C., Zhou, F., Campos-Torres, J., and Leder, P. Pleiotropic defects in ataxia-telangiectasia protein-deficient mice. Proc. Natl. Acad. Sci. USA., *93:* 13084–13089, 1996.
10. Petiniot, L. K., Weaver, Z., Barlow, C., Shen, R., Eckhaus, M., Steinberg, S. M., Ried, T., Wynshaw-Boris, A., and Hodes, R. J. *Recombinase-activating gene* (*RAG*) *2*-mediated V(D)J recombination is not essential for tumorigenesis in atm-deficient mice. Proc. Natl. Acad. Sci. USA., *97:* 6664–6669, 2000.
11. Liao, M. J., and Van Dyke, T. Critical role for Atm in suppressing V(D)J recombination-driven thymic lymphoma. Genes Dev., *13:* 1246–1250, 1999.
12. Herzog, K. H., Chong, M. J., Kapsetaki, M., Morgan, J. I., and McKinnon, P. J. Requirement for Atm in ionizing radiation-induced cell death in the developing central nervous system. Science (Wash. DC), *280:* 1089–1091, 1998.
13. Kuljis, R. O., Xu, Y., Aguila, M. C., and Baltimore, D. Degeneration of neurons, synapses, and neuropil and glial activation in a murine Atm knockout model of ataxia-telangiectasia. Proc. Natl. Acad. Sci. USA, *94:* 12688–12693, 1997.
14. Borghesani, P. R., Alt, F. W., Bottaro, A., Davidson, L., Aksoy, S., Rathbun, G. A., Roberts, T. M., Swat, W., Segal, R. A., and Gu, Y. Abnormal development of Purkinje cells and lymphocytes in *Atm* mutant mice. Proc. Natl. Acad. Sci. USA, *97:* 3336–3341, 2000.
15. Savitsky, K., Bar-Shira, A., Gilad, S., Rotman, G., Ziv, Y., Vanagaite, L., Tagle, D. A., Smith, S., Uziel, T., Sfez, S., Ashkenzi, M., Pecker, I., Frydman, M., Harnik, R., Patanjali, S. R., Simmons, A., Clines, G. A., Sartiel, A., Gatti, R. A., Chessa, L., Sanal, O., Lavin, M. F., Jaspers, N. G. J., Taylor, A. M. R., Arlett, C. F., Miki, T., Weissman, S. M., Lovett, M., Collins, F. S., and Shiloh, Y. A single ataxia-telangiectasia gene with a product similar to P1–3 kinase. Science (Wash. DC), *268:* 1749–1753, 1995.
16. Lavin, M. F., and Khanna, K. K. ATM. The protein encoded by the gene mutated in the radiosensitive syndrome ataxia-telangiectasia. Int. J. Radiat. Biol., *75:* 1201–1214, 1999.
17. Morgan, S. E., Lovly, C., Pandita, T. K., Shiloh, Y., and Kastan, M. B. Fragments of ATM, which have dominant-negative or complementing activity. Mol. Cell. Biol., *17:* 2020–2029, 1997.
18. Watters, D., Khanna, K. K., Beamish, H., Birrell, G., Spring, K., Kedar, P., Gatei, M., Stenzel, D., Hobson, K., Kozlov, S., Farrell, A., Ramsay, J., Gatti, R., and Lavin, M. F. Cellular localization of the ataxia-telangiectasia (*ATM*) gene proteins and discrimination between mutated and normal forms. Oncogene, *14:* 1911–1921, 1997.
19. Pecker, I., Avraham, K. B., Gilbert, D. J., Savitsky, K., Rotman, G., Harnik, R., Fukao, T., Schrock, E., Hirotsune, S., Tagle, D. A., Collins, F. S., Wynshaw-Boris, A., Ried, T., Copeland, N. G., Jenkins, N. A., Shiloh, Y., and Ziv, Y. Identification and chromosomal localization of *Atm*, the mouse homologue of the ataxia-telangiectasia gene. Genomics, *1:* 39–45, 1996.
20. Williams-Simons, L., and Westphal, H. EIIA-Cre-utility of a general deleter strain. Transgenic Res., *8:* 53–54, 1999.
21. Canman, C. E., Lim, D-S., Cimprich, K. A., Taka, Y., Tamai, K., Sakaguchi, K., Appella, E., Kastan, M. B., and Siliciano, J. D. Activation of the ATM kinase by ionizing radiation and phosphorylation of p53. Science (Wash. DC), *281:* 1677–1679, 1998.
22. Zhang, N., Chen, P., Khanna, K. K., Scott, S., Gatei, M., Kozlov, S., Watters, D., Spring, K., Yen, T., and Lavin, M. F. Isolation of full-length ATM cDNA and correction of the ataxia-telangiectasia cellular phenotype. Proc. Natl. Acad. Sci. USA, *94:* 8021–8026, 1997.
23. Ansari, B., Coates, P. J., Greenstin, B. D., and Hall, P. A. *In situ* end-labeling detects DNA strand breaks in apoptosis and other physiological and pathological states. J. Pathol., *170:* 1–8, 1993.
24. Sauer, B., and Henderson, N. Targeted insertion of exogenous DNA into the eukaryotic genome by the Cre recombinase. New Biol., *2:* 441–499, 1990.
25. Khanna, K. K., Keating, K. E., Kozlov, S., Scott, S., Gatei, M., Hobson, K., Taya, Y., Gabrielli, B., Chan, D., Lees-Miller, S. P., and Lavin, M. F. ATM associates with and phosphorylates p53: mapping the region of interaction. Nat. Genet., *20:* 398–400, 1998.
26. Banin, S., Moyal, L., Shieh, S-Y., Taya, Y., Anderson, C. W., Chessa, L., Smorodinsky, N. I., Prives, C., Reiss, Y., Shiloh, Y., and Ziv, Y. Enhanced phosphorylation of p53 by ATM in response to DNA damage. Science (Wash. DC), *281:* 1647–1677, 1998.
27. Taylor, A. M., Harnden, D. G., Arlett, C. F., Harcourt, S. A., Lehmann, A. R., Stevens, S., and Bridges, B. A. Ataxia-telangiectasia: a human mutation with abnormal radiation sensitivity. Nature (Lond.), *4:* 427–429, 1975.
28. Xu, Y., and Baltimore, D. Dual role of ATM in the cellular response to radiation and in cell growth control. Genes Dev., *10:* 2401–2410, 1996.
29. Wilson, A., Capone, M., and MacDonald, H. R. Unexpectedly late expression of intracellular CD3ϵ and TCR $\gamma\delta$ proteins during adult thymus development. Int. Immunol., *11:* 1641–1650, 1999.
30. Westphal, C. H., Rowan, S., Schmaltz, C., Elson, A., Fisher, D. E., and Leder, P. *Atm* and *p53* cooperate in apoptosis an suppression of tumorigenesis but not in resistance to acute radiation toxicity. Nat. Genet., *16:* 397–401, 1997.
31. Simpson, E. M., Linder, C. C., Sargent, E. E., Davisson, M. T., Mobraaten, L. E., and Sharp, J. J. Genetic variation among 129 substrains and its importance for targeted mutagenesis in mice. Nat. Genet., *16:* 19–27, 1997.

32. Nagata, S. Apoptosis by death factor. Cell, *88:* 355–365, 1997.
33. Gatei, M., Scott, S. P., Filippovich, I., Sorokina, N., Lavin, M. F., Weber, B., and Khanna, K. K. Role for ATM in DNA damage-induced phosphorylation of BRCA1. Cancer Res., *60:* 3299–3304, 2000.
34. Bosotti, R., Isacchi, A., and Sonnhammer, E. L. FAT: a novel domain in PIK-related kinases. Trends Biochem. Sci., *25:* 225–227, 2000.
35. Wang, Y., Cortez, D., Yazdi, P., Neff, N., Elledge, S. J., and Qin, J. BASC, a super complex of BRCA1-associated proteins involved in the recognition and repair of aberrant DNA structures. Genes Dev., *14:* 927–939, 2000.
36. Westphal, C. H., Hoyes, K. P., Canman, C. E., Huang, X., Kastan, M. B., Hendry, J. H., and Leder, P. Loss of Atm radiosensitizes multiple p53 null tissues. Cancer Res., *58:* 5637–5639, 1998.
37. Strasser, A., Harris, A. W., Jacks, T., and Cory, S. DNA damage can induce apoptosis in proliferating lymphoid cells via p53-independent mechanisms inhibitable by Bcl-2. Cell, *79:* 329–339, 1994.
38. Barlow, C., Brown, K. D., Deng, C-X., Tagle, D. A., and Wynshaw-Boris, A. Atm selectively regulates distinct p53-dependent cell-cycle checkpoints and apoptotic pathways. Nat. Genet., *17:* 453–456, 1997.
39. Meyn, M. S., Strasfeld, L., and Allen, C. Testing the role of p53 in the expression of genetic instability and apoptosis in ataxia-telangiectasia. Int. J. Radiat. Biol., *66:* 1441–1449, 1994.
40. Brown, J. M., and Wouters, B. G. Apoptosis, p53, and tumor cell sensitivity to anticancer agents. Cancer Res., *59:* 1391–1399, 1999.
41. Wang, Y. A., Elson, A., and Leder, P. Loss of *p21* increases sensitivity to ionizing radiation and delays the onset of lymphoma in *Atm*-deficient mice. Proc. Natl. Acad. Sci. USA, *94:* 14590–14595, 1997.
42. Kischkel, F. C., Hellbardt, S. , Behrmann, I., Germer, M., Pawlita, M., Krammer, P. H., and Peter, M. E. Cytotoxicity-dependent APO-1 (Fas/CD95)-associated proteins form a death-inducing signaling complex (DISC) with the receptor. EMBO J., *14:* 5579–5588, 1995.
43. Chinnaiyan, A. M., Orth, K., O'Rourke, K., Duan, H., Poirier, G. G., and Dixit, V. M. Molecular ordering of the cell death pathway. Bcl2 and Bcl-xL function upstream of the CD-3-like apoptotic proteases. J. Biol. Chem., *271:* 4573–4576, 1996.
44. Lenardo, M. J. Interleukin-2 programs mouse α β T lymphocytes for apoptosis. Nature (Lond.), *353:* 858–861, 1991.
45. Belka, C., Marini, P., Budach, W., Schulze-Osthoff, K., Lang, F., Gulbins, E., and Banberg, M. Radiation-induced apoptosis in human lymphocytes and lymphoma cells critically relies on the up-regulation of CD95/Fas/APO-1 ligand. Radiat. Res., *149:* 588–595, 1998.
46. Xu, X., Fu, X. Y., Plate, J., and Chong, A. S. IFN-γ induces cell growth inhibition by Fas-mediated apoptosis: requirement of STAT1 protein for up-regulation of Fas and FasL expression. Cancer Res., *58:* 2832–2837, 1998.
47. Naujokat, C., Sezer, O., and Possinger, K. Tumor necrosis factor-α and interferon-γ induce expression of functional fas ligand on HT29 and MCF7 adenocarcinoma cells. Biochem. Biophys. Res. Commun., *264:* 813–819, 1999.
48. Hsu, S. C., Gavrilin, M. A., Lee, H. H., Wu, C. C., Han, S. H., and Lai, M. Z. NF-κ B-dependent Fas ligand expression. Eur. J. Immunol., *29:* 2948–2956, 1999.